Arabian Journal of Chemistry (2022) **15**, 103518

King Saud University

Arabian Journal of Chemistry

www.ksu.edu.sa
www.sciencedirect.com

ORIGINAL ARTICLE

Modification in structural, optical, morphological, and electrical properties of zinc oxide (ZnO) nanoparticles (NPs) by metal (Ni, Co) dopants for electronic device applications

Shahroz Saleem [a], Muhammad Hasnain Jameel [b,*], Naheed Akhtar [c], Nousheen Nazir [c], Asad Ali [d], Abid Zaman [d,*], Ateequr Rehman [e], Shoaib Butt [f], Fozia Sultana [g], Muhammad Mushtaq [h], Jing Hui Zeng [a], Mongi Amami [i,j], Khaled Althubeiti [k,*]

[a] *Shaanxi Key Laboratory for Advanced Energy Devices and Shaanxi Engineering Lab for Advanced Energy Technology, Xi'an 710119, China*
[b] *Shaanxi Key Laboratory for Theoretical Physics Frontiers, Institute of Modern Physics, Northwest University, Xi'an 710069, China*
[c] *Institute of Chemical Sciences, University of Peshawar, Peshawar 25000, Pakistan*
[d] *Department of Physics, Riphah International University Islamabad, 44000, Pakistan*
[e] *Department of Physics, University of Agriculture Faisalabad, 38040 Faisalabad, Pakistan*
[f] *College of Physics and Information Technology, Shaanxi Normal University, Xian 710069, Shaanxi, PR China*
[g] *University of Science and Technology of China, Hefei, Anhui 230026, PR China*
[h] *Faculty of Materials Science, Beijing University of Technology, Beijing 100124, PR China*
[i] *Department of Chemistry College of Sciences, King Khalid University, P.O. Box 9004, Abha, Saudi Arabia*
[j] *Laboratoire des matériaux et de l'environnement pour le développement durable LR18ES10, 9 Avenue Dr.Zoheir Sai, 1006 Tunis, Tunisia*
[k] *Department of Chemistry, College of Science, Taif University, P.O. Box 11099, Taif 21944, Saudi Arabia*

Received 1 August 2021; accepted 20 October 2021
Available online 25 October 2021

KEYWORDS

Ni,Co/ZnO;
Crystal Structural;
Microstructure;

Abstract In the present work, Zinc Oxide (ZnO) nanoparticles (NPs) were synthesized by the chemical co-precipitation method using Zinc Chloride as the initial chemical, while Nickel and Cobalt chloride as dopants. Phase identification of metal (Ni, Co) doped Zinc Oxide nanoparticles (NPs) was observed using x-ray diffraction (XRD). The small lattice distortion or phase changes

* Corresponding authors.
E-mail addresses: mhasnainjamil@gmail.com (M.H. Jameel), zaman.abid87@gmail.com (A. Zaman), k.althubeiti@tu.edu.sa (K. Althubeiti).
Peer review under responsibility of King Saud University.

Production and hosting by Elsevier

https://doi.org/10.1016/j.arabjc.2021.103518

UV;
FT-IR spectroscopy;
IV

appeared due to shifting of diffraction angles peaks towards larger angle in ZnO are corresponded to metal (Ni, Co) dopant. The average crystallite size appears to decrement in NP size from 7.67 nm to 6.52 nm and 5.35 nm to 5.17 nm with increasing 5 % to 80 % of metal (Ni, Co) dopant respectively. The optical characteristics, including the absorption spectra of the prepared sample were observed through UV–Vis spectroscopy, Meanwhile SEM confirmed the observation of composition change in specimen with metal (Ni, Co) dopant concentration. The bandgap value was also found decrement 5.23 eV to 5.05 eV with increment of metal (Ni, Co) dopant concentration. The functional groups were measured by Fourier transformation infrared spectroscopy (FTIR). FTIR peaks found the metal (Ni, Co) doped ZnO with the vibration mode of (Zn^{2+} –O^{2-}) ions due to the increment of dopant concentrations. Furthermore, electrical results show the ohmic behavior of prepared samples. These findings indicate the possibility of tuning optical, structural and electrical properties of metal (Ni, Co) doped ZnO with various dopant concentrations of Nickel and will have great potential to find application in optoelectronic devices.

1. Introduction

Metal (Ni, Co) doped Zinc Oxide is one of the distinct inorganic semiconductor material which has a wide direct bandgap (3.37 eV) and a large exciton binding energy of 60 meV at a room temperature based on the wurtzite-structured and oxygen vacancies. Among the various semiconductor materials, Zinc Oxide has achieved wide interest in the research field due to its remarkably larger bandgap, low synthesis cost, easy availability, high photosensitivity, high electrochemical stability, electro-optical properties and high biocompatibility (Vafaee and Ghamsari, 2007; Vijayaprasath et al., 2016; C. Belkhaoui, N. Mzabi, and H. Smaoui, "Investigations on structural , optical and dielectric properties of Mn doped ZnO nanoparticles synthesized by co-precipitation method," Materials Research Bulletin, vol. 111, no. October 2018; Prasad et al., 2015; Bilecka et al., 2011). It has also established significant consideration for materials researchers because of its promising properties and numerous uses in several potential applications. This include light-emitting diodes, heat mirrors, optoelectronic devices, ultraviolet photoconductive devices, surface acoustic wave devices (SAW), laser devices, solar cell transparent, piezoelectric devices, varistors and gas sensor devices. Metal (Ni, Co) doped Zinc Oxide has several properties, including size-dependent physical properties, electrical properties, optical and mechanical properties which depend on the size, synthesis technique and structure of prepared Zinc Oxide nanoparticles (NPs) (Giovannelli et al., 2014; Ghotbi, 2012).

Among several inorganic semiconductors, several physical and chemical methods have synthesized a wide variety of Zinc Oxide micro/nanostructures, including rods, tubes, wires, belt, cages, flowers or rings. This includes co-precipitation process, hydrothermal process, microwave irradiation, pulsed laser deposition, solid-state reaction process, sol–gel process, spray pyrolysis technique, solution combustion, mechanical ball milling and microwave-assisted solvo-thermal methods (Giovannelli et al., 2014). The sol–gel process has a major disadvantage, however it provides fine magnetic nanoparticles of more non-homogeneous composition, also provides a better control ratio and is also a simple preparation technique. But, stoichiometry is lost during filtering steps in this technique. Among these methods, the co-precipitation process gained more attention due to its exceptional advantages including large-scale preparation of nanoparticles (NPs), simple lab equipment, and simplicity in itself, low cost, effective and easy adjustment of dopant concentration (Kumar et al., 2016; Khorsand et al., 2016).

Several literatures have been reported about the study the of effect of different metal dopants on different parameters of synthesized Zinc Oxide (ZnO) nanoparticles (NPs) by using numerous techniques. However, there existed some defects for ZnO. In terms of crystallinity, functional group, surface morphology and band gap energy, Ghotbi (Ghotbi, 2012) found that 4 % Nickel doped ZnO nanoparticles (NPs) synthesized by hydrothermal method exhibited crystallite size of 27.6 nm, broad-band at 3372 cm^{-1}, thin flake-like micro size sheets. It is to be expected from the layer materials and energy gap by 3.25 eV (Ghotbi, 2012). On the other Kumar *et al*. found that 10 % of Cobalt doped ZnO nanoparticles (NPs) by chemical precipitation route exhibited crystallite size of 45.14 nm, broad-band at 3348 cm^{-1}, band gap energy of 3.13 eV and rode like nanostructure that can be possible for nano-layer materials. But it is not for nanoparticles (NPs) (Yildiz et al., 2019). Ali Khorsand *et al*. reported that Ga doped ZnO nanoparticles (NPs) prepared by gelatin based sol–gel approach showed that increasing the concentration of Ga dopant yields the crystallite size as 12.2 nm and band gap energy of 3.42 eV (Ozel and Yildiz, 2021; Raja et al., 2019).

The different metals doped ZnO nanoparticles (NPs) were prepared in this study by co-precipitation method. They were doped with various concentrations of Nickel and Cobalt metals dopants. In this work, the influence of different dopants (Co and Ni) is varied by their concentrations on the crystallite size, particle size, energy band gap and functional group for tuning the optical, electrical, morphological, functional and structural properties of electrical, optoelectronic and energy storage devices. The crystallinity, morphology, absorbance, functionality and electrical conductivity of metals doped ZnO nanoparticles NPs were analyzed by XRD, SEM, UV-spectra, FT-IR and IV analyses. Finally, the ZnO sample doped with 50 % Cobalt exhibited absorbance at 353 nm, 5.05 nm ultra-wide band gap energy, 3.70 % porosity, 5.17 nm crystallite size and 3383.13 cm^{-1} OH stretching vibrations. This, as smaller than that of the sample doped with 25 % Cobalt, 25 % nickel and 50 % Nickel. The lowest obtained absorption spectra, crystallite size, porosity, band gap energy and stretching vibration are with 25 % Cobalt doped ZnO sample, which suggested its potential use as an optoelectronic or photo- conductive device.

2. Experimental procedure

2.1. Sample preparation

The samples of (X-Y-ZnO) (X = Nickel, and Y = Cobalt) with X, Y varying concentrations of Ni, Co from 5–80 % were synthesized by the chemical co-precipitation technique. Zinc Chloride ($ZnCl_2$) and Sodium Hydroxide (NaOH) were used as initial chemicals, while Nickel Chloride ($NiCl_2$) and Cobalt Chloride ($CoCl_2{\cdot}6H_2O$) were involved as metal dopants; their concentrations were weighted by electric balance. Here deionized water was taken as solvent. 5 % Nickel dopant and 95 % Zinc Chloride ($ZnCl_2$) were dissolved into deionized water. Both solutions were separately stirred for 30 min and

combined into a solution. Furthermore, this combined solution was kept on a magnetic stirrer for 1 h. 100 mL Sodium Hydroxide solution was added drop by drop into this solution during stirring. The (NaOH) solution was added until the pH value of the solution reached 7. The pH of the solution becomes neutral at 7. But the solution would become basic if the pH is more than 7. Therefore the pH of the solution must be maintained at 7. The solution turns into light green in color was obtained at the end. After that, the prepared light green colored solution was stirred for 1 h, so that the homogeneity of the prepared solution could be maintained. At the beaker's bottom, elements of light green color were established. The particles were washed with distilled water. After washing and filtration the final product was placed in a china dish and dehydrated for 2 h in an oven at 90 °C to get rid of the remaining water. After washing and filtration, a powdered form sample was obtained. To produce extra fine precipitates, the final sample was grinded and at four hours heated at 500 °C in a furnace. The prepared samples of Ni-doped ZnO were cooled down. Similarly, three further samples were synthesized by using different concentrations of initial chemical and metal dopants. In the second sample, 80 % Nickel Chloride ($NiCl_2$) and 20 % Zinc Chloride ($ZnCl_2$) were kept. In third sample, 5 % Cobalt chloride ($CoCl_2{\cdot}6H_2O$) and 95 % zinc chloride ($ZnCl_2$) were kept. In forth, 80 % Cobalt Chloride ($CoCl_2{\cdot}6H_2O$) and 20 % Zinc chloride ($ZnCl_2$) were kept. The synthesized metals doped Zinc Oxide nanoparticles (NPs) were characterized to examine their morphology and micro structure, formation, chemical composition, surface and electrical characteristics by utilizing Scanning electron microscopy,
X-ray diffraction, UV–visible spectroscopy, FTIR and I-V.

3. Results and discussion

3.1. Phase analysis

X-ray diffraction (XRD) patterns were recorded by a Philips X-ray diffractometer using Ni-filtered CuKα radiation. The XRD patterns which with (0.05 and 0.8) of Nickel and (0.05 and 0.8) Cobalt are shown in Fig. 1. All the samples showed the hexagonal wurtzite phase which was confirmed by XRD analysis. Crystallite sizes calculated were 7.67 nm, 6.52 nm, 5.35 nm and 5.17 nm for ZnO nanoparticles NPs doped with metals Nickel and Cobalt (Ni, Co) 0.05 and 0.2 respectively. The crystallite sizes were decreased by increasing the concentration of dopants in samples. No impurity peaks were observed, which indicated that four samples of ZnO doped with metals Nickel and Cobalt (Ni, Co) nanoparticles (NPs) were highly pure which revealed good crystalline in the nature of the samples. By increasing the concentrations of dopants, the characteristic peak was shifted toward a higher angle. The main peak which showed analyzed sample Cobalt were at higher angle and its full width at high maximum was higher as compared to that of other samples doped with 0.05 Nickel, 0.2 Nickel and Cobalt. It also indicated that the crystallite size was 5.17. These results revealed that crystallite size was highly decreased by doping with 0.05 Cobalt.

XRD analysis was carried out to determine the structural properties, such as phase formation and crystal structure of the prepared product. Debye-Scherrer equation was used to calculate the crystallite size of nanoparticles (NPs) (Ragupathi et al., 2015; Zaman et al., 2020).

$$D = \frac{K\lambda}{\beta Cos\Theta} \tag{1}$$

Where D is crystallite size, θ is the Bragg diffraction angle, β is the FWHM of the XRD peak appearing at the diffraction angle θ and where λ is the X-ray wavelength (Cu Kα radiation equals to 1.54 Å) The inter-planner spacing or d-spacing was corresponding to (1 0 1) characteristic peak was determined by Bragg's law formula which was given as (Jameel et al., 2020).

$$d = \frac{\lambda}{2\sin\theta} \tag{2}$$

Where 'd' is d-spacing λ is the X-ray wavelength (Cu Kα radiation equals 1.54 Å) and θ is the Bragg diffraction angle.

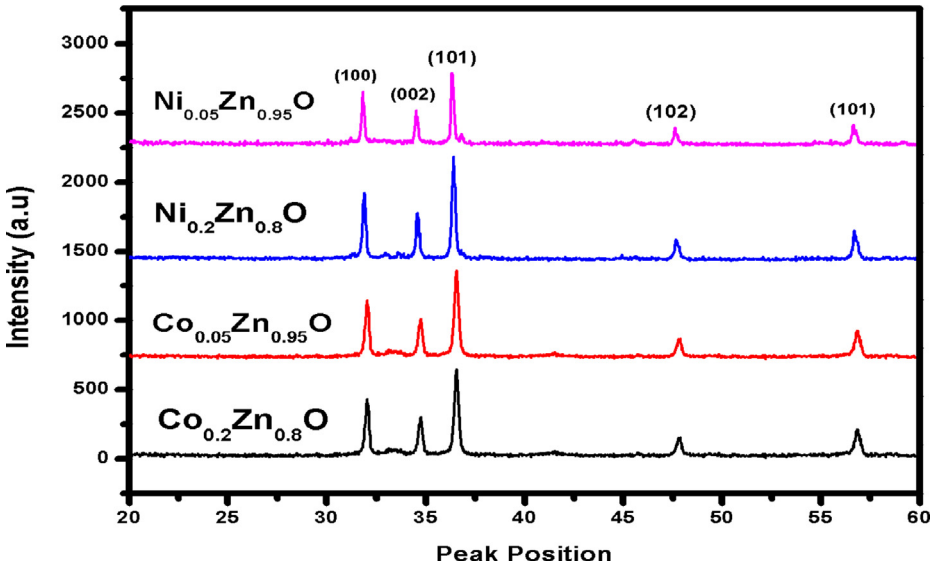

Fig. 1 XRD Spectra of metal dopant (Ni, Co) ZnO nanoparticles (NPs).

Table 1 Lattice Parameters of metal dopant (Ni, Co) ZnO nanoparticles NPs.

Samples	Crystallite Size (D) (nm)	d-spacing	Lattice constant (Å)		Lattice Volume	X-ray density g/cm^3	Bulk Density g/cm^3	Porosity (%)	Williamson-Hall Analysis (ε) (10^{-3})
$Ni_{0.05}Zn_{0.95}O$	7.67	2.4695	2.8361	1.4112	9.8367	6.5850	5.9882	9.06	2.52
$Ni_{0.80}Zn_{0.2}O$	6.52	2.4655	2.8397	1.4117	14.8721	6.6099	6.0720	8.13	3.72
$Co_{0.05}Zn_{0.95}O$	5.35	2.4592	3.2210	1.7610	16.9555	7.5358	7.1189	5.53	5.67
$Co_{0.80}Zn_{0.2}O$	5.17	2.4561	3.2227	1.7623	17.0197	11.3936	10.9715	3.70	8.43

Both lattice constants 'a' and 'c' values increased slightly due to the increased incorporation of Ni and Co in the ZnO nanoparticles (NPs). Therefore a regular increase in cell volume (V_{cell}) (Table 1) with the increase in the content of Ni^{2+} and Co^{2+} ions in composition in the crystal structure is attributed to the increase in lattice constant. Moreover, it can also be seen clearly for the unit cell volume formula, with the increase in the value of 'a' and 'c' cause in the value of unit cell volume to increase. Table 2.Table 4.

$$\frac{1}{d_{hkl}^2} = \frac{4}{3}\frac{h^2+hk+k^2}{a^2} + \frac{l^2}{c^2} \tag{3}$$

Where'd' is d-spacing, h,k,l. are miller indices and a, c are lattice constants.

$$V = \frac{\sqrt{3}}{2}a^2c \tag{4}$$

Where 'V' is unit cell volume and a,c are lattice constants. Moreover

the X-ray density (ρ_{XRD}) of the samples was calculated using the following formula (Jameel et al., 2021).

$$\rho_{XRD} = \frac{8M}{NV} \tag{5}$$

where 'M' is molecular mass, N is Avogadro's number and 'V' is unit cell volume.

The lowest X-ray density exhibited by $Ni_{0.2}$-$Zn_{0.8}O$ was 6.58, which increased with increasing concentrations of dopants up to 11.39. The bulk density (ρ_B) of the samples was calculated by using the following formula

$$\rho_B = \frac{m}{V} \tag{6}$$

The highest bulk density exhibited by $Ni_{0.2}$-$Zn_{0.8}O$ was 5.98, which decreased with increasing concentrations of dopants was up to 10.97. The porosity of the samples was calculated by using the following formula (Arif, 2021).

$$\text{Porosity} = \left(1 - \frac{\rho B}{\rho x}\right) \times 100\% \tag{7}$$

Table 2 Dislocation density of metal dopant (Ni, Co) ZnO nanoparticles (NPs).

Samples	Dislocation Density
$Ni_{0.05}Zn_{0.95}O$	0.016998
$Ni_{0.80}Zn_{0.2}O$	0.023523
$Co_{0.05}Zn_{0.95}O$	0.034937
$Co_{0.80}Zn_{0.2}O$	0.037412

where ρ_B is bulk density and ρ_x is X-ray density.

The calculated value of lattice parameters of four samples were (a = 3.2227, a = 3.2210 and c = 1.7623, c = 1.7610) and (a = 2.8397, a = 2.8361 and c = 1.4117, c = 1.4112).

It is observed that increasing the concentrations of dopants increases the values of 'a' and 'b' lattice parameters. This is attributed to a small mis-match between Zn ion and Ni, Co ions. It indicates that Ni and Co ions systematically substituted Zn ions in the samples without changing their crystal structure. The analyzed lattice volumes of all four samples were 17.0197, 16.9555, 14.8721 and 9.8367. It was noted that this decrease in the lattice volume of unit cell was due to the increase in the concentration of both dopants.

3.2. Dislocation density

The addition of dopants produces the dislocation density, and the dislocation density of the highest peak in all samples was calculated using the equation is given below (Zaman et al., 2021).

$$\delta_{hkl} = \frac{1}{D^2} \tag{8}$$

Where 'δ_{hkl}' is dislocation density and 'D' is crystallite size.

It found from the calculated values $\delta_{hkl} = \frac{1}{D^2}$ data that dislocation density with increase the concentrations dopants in samples. The smallest dislocation density 0.016998 was exhibited by $Ni_{0.05}Zn_{0.95}O$, while highest dislocation density 0.37412 was exhibited by $Co_{0.80}Zn_{0.2}O$. The increase in $\boldsymbol{\delta}_{(hkl)}$ value is caused by the atoms of dopants settled inside the host ZnO matrix. Further, the addition of dopants concentration cause to move from grain boundary to crystallite. So, the increase in $\boldsymbol{\delta}_{(hkl)}$ by increasing dopants concentration may also due to the movement of Ni and Co atoms from grain boundary to crystallite.

3.3. Micro-strain

The effect of microstrain and crystallite size in peak broadening was separated using Williamson-Hall (W-H) plot method (Rajesh Kumar and Hymavathi, 2017).

$$\beta_{hkl}\cos\theta = \frac{K\lambda}{D} + 4\varepsilon \mathrm{Sin}\theta \tag{9}$$

where 'β' is FWHM, 'ε' is strain, 'D' is the crystallite size and 'λ' is wavelength. Accordingly, the variations of $\beta Cos\theta$ with $Sin\theta$ are plotted in Fig. 2, for all the samples.

The equation used to find out the microstrain is given below (Jacob et al., 2017; Chattopadhyay et al., 2021; Ismail et al., 2019).

$\varepsilon = \beta/4tan\theta(a)$

where 'ε' is micro-strain, 'β' is FWHM and 'θ' is the Bragg diffraction angle.

In the Williamson-Hall plot, the plots of $\beta_{hkl}\cos\theta$ versus 4Sinθ is a straight line for the samples doped with 5% and 80% Nickel and Cobalt as shown in Fig. 2. The root of the y-intercept gives micro-strain, while the crystallite size is determined from the slope of the linearly fitted data. All the values of micro-strain indicate that the prepared samples are under tensile strain. The calculated values of strain (ε) are 2.2591×10^{-3}, $3.7246\text{x}10^{-3}$, $5.6711\text{x}10^{-3}$ and $8.4304\text{x}10^{-3}$ of ZnO doped with metals Nickel and Cobalt (Ni, Co) nanoparticles (NPs), respectively also represented in Table 3. The micro-strain results exhibit an opposite trend to the crystallite size, such as micro-strain increased with increase in the concentrations of metal (Ni, Co) dopants. The highest crystallite nanoparticles NPs exhibited smaller micro-strain, while the smallest nanoparticles (NPs) exhibited higher micro-strain. Furthermore, the increase in micro-strain may be due to the growth of smaller grains of metals-doped ZnO with respect to an increase in concentrations of dopants. Hence, it showed that the influence of doping of Ni and Co on the average crystallite size and microstrain for as-prepared samples is investigated.

3.4. Morphological analysis

The shape and surface morphology of the synthesized metals doped ZnO nanoparticles (NPs) were analyzed using scanning

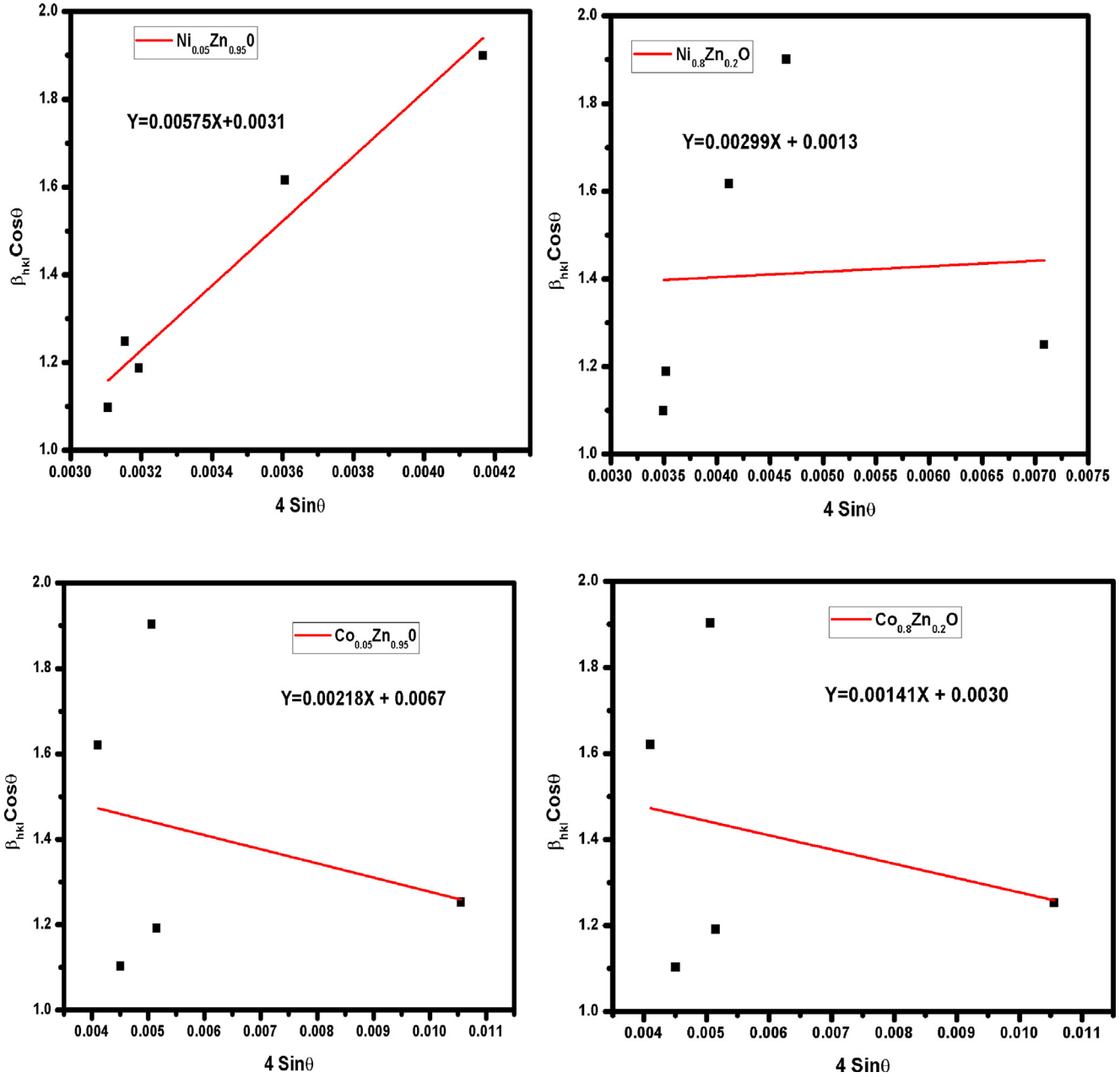

Fig. 2 Williamson-Hall plots of metals of dopant (Ni, Co) ZnO nanoparticles NPs.

Table 3 Band gap for metal dopant (Ni, Co) ZnO nanoparticles NPs.

Samples	Absorption wavelength (nm)	Band gap (eV)
$Ni_{0.05}Zn_{0.95}O$	365	5.23
$Ni_{0.80}Zn_{0.2}O$	361	5.19
$Co_{0.05}Zn_{0.95}O$	356	5.13
$Co_{0.80}Zn_{0.2}O$	351	5.05

electron microscopy. Fig. 3. exhibit the surface morphology of the ZnO nanoparticles (NPs) under different magnifications. The SEM image showed that most nanoparticles (NPs) are spherical formed within a diameter of 80–130 nm. The sample of ZnO which was doped with 20% Nickel showed non-uniform distribution and irregularly shaped particles. The surface morphology was gradually changed by increasing the concentration of dopants. The sample was doped with 80% Nickel small in particle size, shape and morphology. 20% nickel doped ZnO nanoparticles (NPs) showed the small agglomera-

Table 4 FTIR spectra with possible assignments.

Frequency (cm)				Possible Assignment
Ni-doped ZnO		Co-doped ZnO		
3397.65	3395.44	3390.31	3386.13	OH Stretching Vibrations
2933.45	2927.65	2922.57	2912.41	The C-H stretch in alkanes
2880.49	2870.33	2859.45	2849.29	O-H stretch in carboxylic acid
1718.12	1712.37	17027.29	1697.13	C = C stretch in aromatic ring and C = O
1461.33	1456.26	1440.29	1424.33	C-N stretch of amide-1 in protein
1100.06	1094.09	1085.49	1078.96	C-O stretching in amino acid
612.45	602.30	597.22	591.41	Hexagonal phase ZnO

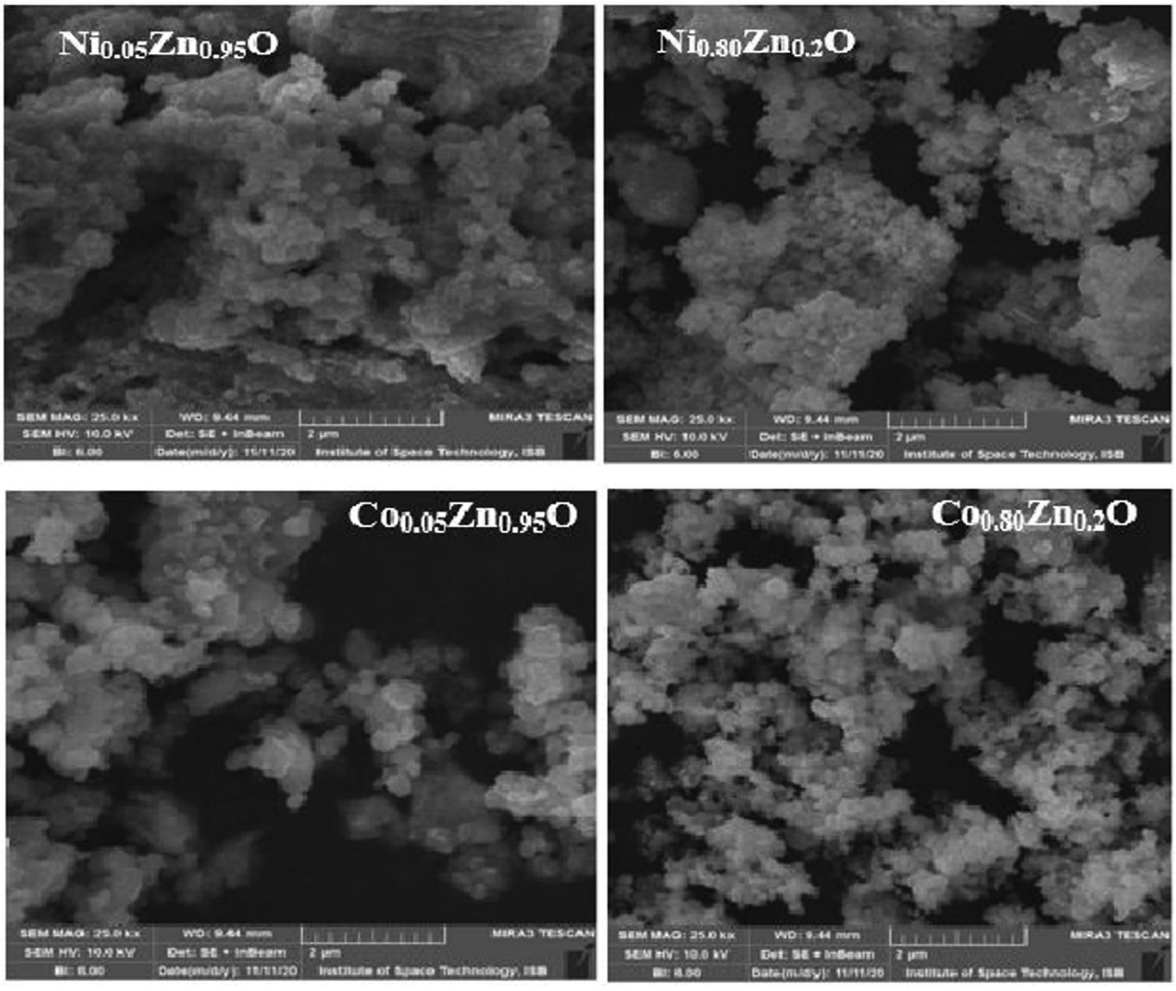

Fig. 3 SEM micrographs of metal dopant (Ni, Co) ZnO nanoparticles NPs.

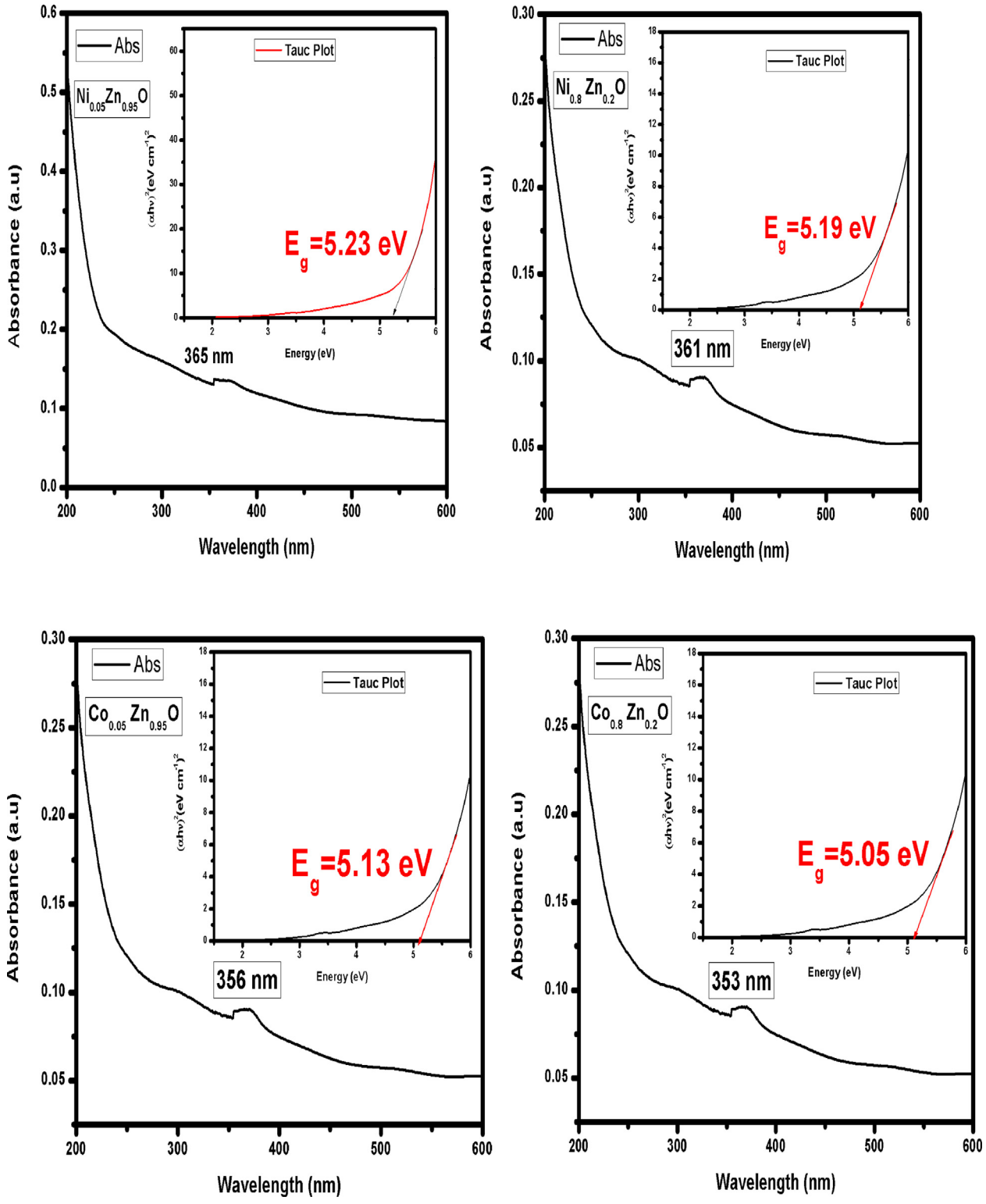

Fig. 4 UV–Visible Absorption Spectra of metal dopant (Ni, Co) ZnO nanoparticles NPs.

tion, non-uniform distribution and 9.06 % porosity. With increasing the concentration of nickel from 20% to 80%, the agglomeration was slightly increased, non-uniformly distributed nanoparticles (NPs) and 8.13 % porosity. Some particles are also found in bunches due to agglomeration. The ZnO doped with 20% Cobalt showed a highly uniform distribution, moderate agglomeration and 5.53% porosity. By increasing the concentration of Cobalt from 20% to 80%, the agglomeration was highly increased, highly non-uniformly distributed nanoparticles (NPs) and 3.70% porosity. It is important to

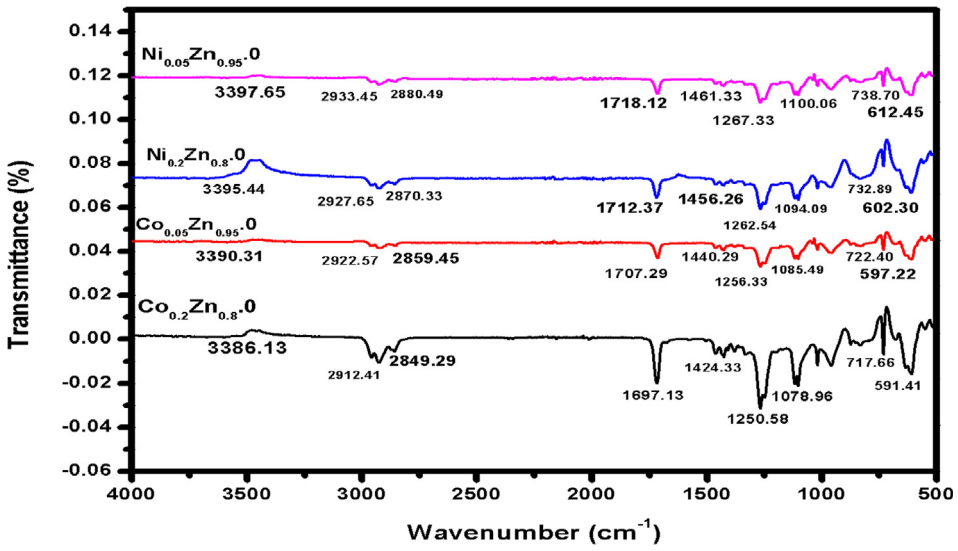

Fig. 5 FTIR Spectra of metal dopant (Ni, Co) ZnO nanoparticles NPs.

note that porosity was decreased from 9.06% to 3.70% with increasing the concentrations of dopants. The SEM micrographs of metals doped ZnO samples are given in Fig. 3.

3.5. UV visible

UV–Vis absorption calculations along with the band gap measurement with 5% and 80% concentrations of metal (Ni, Co) doped ZnO are shown in Fig. 4. The absorption measurements have been carried out in the range of 200–800 nm. The prepared $Ni_{0.05}Zn_{0.95}O$, $Ni_{0.8}Zn_{0.2}O$, $Co_{0.05}Zn_{0.95}O$ and $Co_{0.8}Zn_{0.2}O$ samples exhibited absorption peaks at 365 nm, 361 nm, 356 nm and 353 nm, respectively which are the characteristic absorption peaks for wurtzite hexagonal Zinc Oxide. Prominent redshift appeared for metal-doped ZnO nanoparticles (NPs) corresponding to increasing dopant concentrations (Abbas et al., 2021; Parra and Haque, 2014; Vijayakumar et al., 2018; Jameel et al., 2021). Using Tauc's equation, the energy band gap of doped samples can be calculated through the extrapolation line in the plot of $(\alpha hv)^n$ given by;

$$(\alpha hv) = k\left(hv - E_g\right)^n \tag{10}$$

where "α" is the absorbance coefficient, "hv" is the incident photon energy, "k" is the energy independent constant while "E_g" is the energy gap of the optical band. The band gap values were obtained using the Tauc plot by plotting the energy of the absorbed light against the Kubelka–Munk function. The standard band gap value for ZnO is 3.3 eV, but ZnO doped with 5% and 80% Nickel exhibited the wide band gap of 5.23 eV and 5.19 eV, respectively. Moreover ZnO doped with 5% and 80% Cobalt exhibited 5.13 eV and 5.05 eV, respectively. The band gap value in the range of 5.23 to 5.05 eV was considered an ultra-wide band gap semiconductor material. These higher band gaps are due to the too high energy of conduction band minimum (CBM), which nearly equal to the reported band gap of ZnO in the reports (Fan and Freer, 1993; Alhadhrami et al., 2018). Due to the higher band, ZnO NPs exhibited high resistivity and lower conductivity. However, when high energy of conduction band minimum (CBM) records a slight decrease causes the band gap to decrease from 5.23 eV to 5.05 eV, As a result resistivity also decreased. Furthermore, conductivity is also slightly increased.

Although; the standard band gap of ZnO is 3.3 eV, those nanomaterials with a have band gap of about 3.3 eV are considered as a semiconductor. However, in the current study ZnO nanoparticles (NPs) have an ultra-wide band gap of 5.23 eV, 5.19 eV, 5.13 eV and 5.05 eV, with electronic properties, which fall between conventional semiconductor and insulators. The higher energy gap gives devices the ability to operate at higher temperatures and power-switching. Furthermore, the band gap shrinks with increasing temperature. Thus, wide band gap semiconductors are useful at shorter wavelengths than other semiconductor materials.

3.6. Fourier transformation infrared spectroscopy (FTIR)

FT-IR is an effective method to reveal the composition of products and helps in indentifying the possible fuinctional groups involved in Ni-doped ZnO and Co-doped nanoparticles (NPs). This spectrum is a powerful technique that is used to probe different ordering phenomena. This technique provides the information about the crystal vibration modes and the position of ions in the crystal. The FTIR spectra of metal (Ni, Co) doped ZnO nanoparticles (NPs) are represented in Fig. 5. The spectrum obtained clearly showed the ZnO absorption band in the range between 550 cm^{-1} and 650 cm^{-1}. The FTIR analysis was performed in the frequency range of 500 cm^{-1} to 4000 cm^{-1} at room temperature. A peak at 612 cm^{-1} is the characteristic absorption of the Zn-O bond which is shifted towards 602 cm^{-1}, 597 cm^{-1} and 591 cm^{-1} due to the varation or increasing concentrations of Cobalt (Co) and Nickel (Ni) dopant in other samples. This band shows that the materials are Nickel doped Zinc Oxide and Cobalt doped Zinc Oxide (Mohamed and Khairalla, 2019; Wahab et al., 2008; Srivastava et al., 2013). The broad absorption peak at 3397 cm^{-1} can be attributed to the characteristic absorption of hydroxyl groups (O-H). Due to the increase in concentrations of both dopants, this broad absorption peak

was shifted towards 3395 cm^{-1}, 3390 cm^{-1} and 3386 cm^{-1}. These data are similar to the results observed by others . Peaks 1718.12 cm^{-1}, 1712.37 cm^{-1}, 1707.29 cm^{-1} and 1697.13 cm^{-1} were due to the bending of water molecules. The bands at 1461.33 cm^{-1}, 1456.26 cm^{-1}, 1440.29 cm^{-1} and 1424.33 cm^{-1}. The spectrum showed bands at stretching of alkanes, C-H (aromatics), C = C-H (alkynes) and –OH stretching in intermolecular H-bond, C = O and C-C stretching of alkanes (5). Some unresolved peaks in precipitate may be due to some impurities (Kumar and Choubey, 1512; Singh et al., 2020; Nava et al., 2017). Fig. 6.

3.7. Current voltage (I-V) characteristics

From the I-V curves, a linear behavior can be seen implying the ohmic nature of the prepared Ni, Co-ZnO sample. The resistivity and conductivity of the Ni, Co-ZnO were calculated using the following equation:

$$\rho = \mathscr{R}bt/l \tag{11}$$

where R is the resistance of the sample, b is the width of the electrodes; t is the thickness of the sample and l is the length of the electrodes. The conductivity of the material was calculated by taking the inverse of the resistivity. I-V characteristic curves show the relationship between the current flowing through an electronic device and the applied voltage across its terminals. Thus optimization of proton conductivity depends on the proton transport, defect formation and chemical stability of the materials. The determination of proton conductivity relies on the introduction of defects into the oxide structure and their distribution in the crystalline lattice. The proton conductivity is dependent on the concentration of oxygen vacancies in the oxides producing reactive sites and enabling ionic diffusion. When the material is exposed to hydrogen rich or hydroxyl group filled the oxygen vacancies, simply that protons are combined into perovskite structure leading to proton defect (Yedurkar et al., 2016; Ali et al., 2021; Grinevich and Filevska, 2020; Kumar et al., 2015; Kumar et al., 2019).

I-V characteristic curves are used to define its operation within an electrical circuit. As its name suggests, I-V characteristic curves show the relationship between the current flowing through an electronic device and the applied voltage across its terminals. I-V characteristic curves are generally used as a tool to determine and understand the basic parameters of a component or device. They can also be used to mathematically model its behavior within an electronic circuit. But as with most electronic devices, Infinite I-V characteristics curves represent the various inputs or parameters. We can display a family or group of curves on the same graph to represent the various values. For example the electrical supply voltage V, applied to the resistive element R above terminals was varied, the resulting current, can be measured. This current would be characterized as: I = V/R, being one of Ohm's Law equations. Many electronic components and devices which have non-linear characteristics that is their V/I which ratio is not constant. For example non-linear current–voltage characteristics characterized semiconductor diodes as the current flowing through a forward-biased common silicon diode is limited by the ohmic resistance of the PN-junction (Kumar et al., 2019; Panwar et al., 2014; Mondal et al., 2013; Ali et al., 2021).

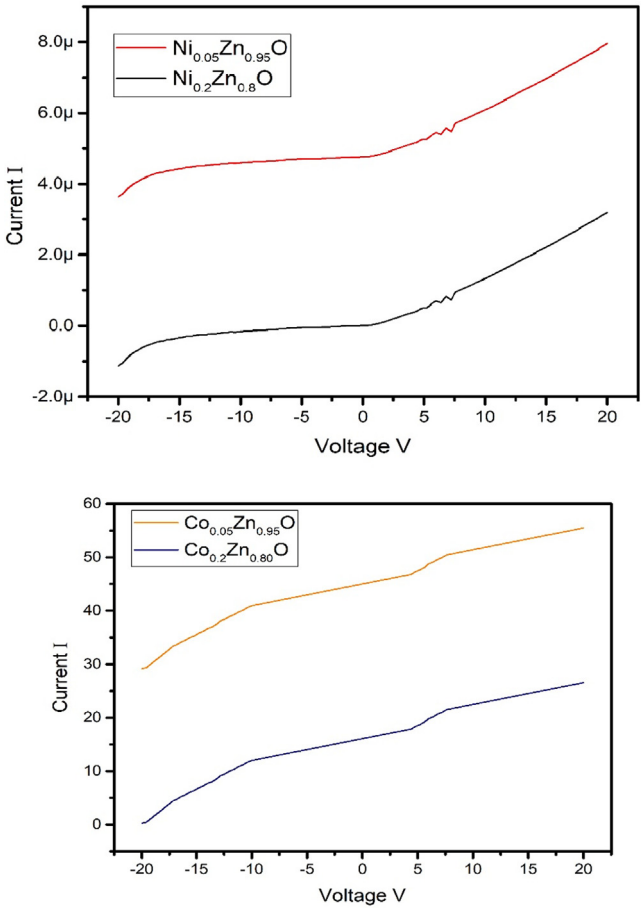

Fig. 6 Current voltage (I-V) characteristics of metal dopant (Ni, Co) ZnO nanoparticles (NPs).

4. Conclusion

In the present work, Zinc Oxide (ZnO) nanoparticles NPs were synthesized by the chemical co-precipitation method by using Zinc Chloride as initial chemical, while Nickel and Cobalt Chloride as dopants. Phase identification of metal (Ni, Co) doped zinc oxide nanoparticles NPs was observed using x-ray diffraction (XRD). The small lattice distortion or phase changes appeared due to shifting of diffraction angle peaks towards larger angle in ZnO are corresponded to metal (Ni, Co) dopant. The average crystallite size appears to decrement in NP size from 7.67 nm to 6.52 nm and 5.35 nm to 5.17 nm with increasing 5 % to 80 % of metal (Ni, Co) dopant respectively. The optical characteristics, including the absorption spectra of prepared sample were observed through UV–Vis spectroscopy, while SEM confirmed that the observation of composition change in specimen with metal (Ni, Co) dopant concentration. The band gap value was also found decrement 5.23 eV to 5.05 eV with increment of metal (Ni, Co) dopant concentration. The functional groups were measured by Fourier transformation infrared spectroscopy (FTIR). FTIR peaks were found metal (Ni, Co) doped ZnO that vibration mode of (Zn^{2+} –O^{2-}) ions due to increment of dopant concentrations. Furthermore, electrical results show that ohmic behavior of prepared sample. These findings indicate possibility of tuning optical, structure and electrical properties of metal (Ni, Co) doped ZnO with various dopant concentrations of nickel and dopant and have great potential to find application in optoelectronic devices.

Declaration of Competing Interest

The authors declare that they have no known competing financial interests or personal relationships that could have appeared to influence the work reported in this paper.

Acknowledgment

Taif University Researchers Supporting Project number (TURSP-2020/241), Taif University, Taif, Saudi Arabia. The authors acknowledges to extend their appreciation to the Deanship of Scientific Research at King khalid University, Saudi Arabia for funding this work through Research Groups Program under grant number R.G.P.1: 43/42.

References

Abbas, M., Ullah, R., Ullah, K., Sultana, F., Mahmood, A., Mateen, A., ... & Zaman, A. Structural, optical, electrical and dielectric properties of (Sr1-xMgx)(Sn0. 5Ti0. 5) O3 (X= 0.00, 0.25, 0.50, 0.75) ceramics via solid state route. Ceramics *International*, *47*(21), 30129-30136 (2021).

Alhadhrami, A., Almalki, A.S., Adam, A.M.A., Refat, M.S., 2018. Preparation of semiconductor zinc oxide nanoparticles as a photocatalyst to get rid of organic dyes existing factories in exchange for reuse in suitable purpose. Int. J. Electrochem. Sci 13 (7), 6503–6521.

Ali, M. H. Jameel, S. Uddin, A. Zaman, Z. Iqbal, Q. Gul, F. Sultana, M. Mushtaq, K. Althubeiti, and R. Ullah, "The Effect of Ca Dopant on the Electrical and Dielectric Properties of BaTi4O9 Sintered Ceramics", *Materials*, *14*(18), 5375, 2021.

A. Ali, S.Uddin, Z.Iqbal, M.Lal, M.H.Jameel, A.Zaman, A.Ahmed and W.Khan, "Synthesis and characterizations of (Ba 1-x Ca x) Ti 4 O 9 , 0 ≤ x ≤ 0 . 9 ceramics," *Journal of Materials Research and Technology*, pp. 2–7, 2021.

M. Arif, M.H. Jameel, M.Q.Hamzah, M.S.Roslan, and S.Z.Haider. Rizvi "Co-precipitation Method in Synthesis and Characterization of BiFeO 3 Doped with Various Concentrations of Mn Nanoparticles for Electronic Device Applications," *Test Engineering and Management*, no. 22302, pp. 22302–22309.

C. Belkhaoui, N. Mzabi, and H. Smaoui, "Investigations on structural , optical and dielectric properties of Mn doped ZnO nanoparticles synthesized by co-precipitation method," *Materials Research Bulletin*, vol. 111, no. October 2018, pp. 70–79, 2019.

Bilecka, I., Luo, L., Djerdj, I., Rossell, M.D., Jagodic, M., Jaglicic, Z., Niederberger, M., 2011. Microwave-assisted nonaqueous sol– gel chemistry for highly concentrated ZnO-based magnetic semiconductor nanocrystals. The Journal of Physical Chemistry C 115 (5), 1484–1495.

Chattopadhyay, S., Kumawat, A., Misra, K.P., Halder, N., Bandyopadhyay, A., Antony, A., Poomaesh, P., Ozgaand, K., Kucharska, B., 2021. Materials Science & Engineering B Microstrain administered SHG intensity enhancement by heavy Ce doping in co-precipitated ZnO nanoparticles. Mater. Sci. Eng., B vol. 266, no. January, 115041.

Fan, J., Freer, R., 1993. The electrical properties and d. c. degradation characteristics of silver doped ZnO varistors. Journal of materials Sciences 83, 1391–1395.

Ghotbi, M.Y., 2012. Particuology Nickel doped zinc oxide nanoparticles produced by hydrothermal decomposition of nickel-doped zinc hydroxide nitrate. Particuology 10 (4), 492–496.

Giovannelli, F., Ndimba, A.N., Diaz-Chao, P., Motelica-Heino, M., Raynal, P.I., Autret, C., Delorme, F., 2014. Synthesis of Al doped ZnO nanoparticles by aqueous coprecipitation. Powder Technol. 262, 203–208.

Grinevich, V., Filevska, L.M., 2020. ELECTROPHYSICAL PROPERTIES OF ZINC OXIDE THIN FILMS OBTAINED BY. Photonics 73, 10–18.

Ismail, A.M., Menazea, A.A., Kabary, H.A., El-sherbiny, A.E., Samy, A., 2019. The in fl uence of calcination temperature on structural and antimicrobial characteristics of zinc oxide nanoparticles synthesized by Sol e Gel method. J. Mol. Struct. 1196, 332–337.

Jacob, A.A., Balakrishnan, L., Shambavi, K., Alex, Z.C., 2017. Multiband visible photoresponse study of Co 2+ doped ZnO nanoparticles. RSC Adv. 7 (63), 39657–39665.

Jameel, M.H., Hamzah, M.Q., Arif, M., Agam, B., 2020. Synthesis and Characterizations of Co-Doped TiO 2 Nanoparticles Via Co-Precipitation Method. Solid State and Technology 4 (September).

Jameel, M.H., Saleem, S., Hashim, M., Roslan, M.S., Somaily, H.H. N., Hessin, M.M., El-Bahy, Z.M., Ashiq, M.G.B., Hamzah, M.Q., Jabbar, A.H., Yabagi, J.A., 2021. A comparative study on characterizations and synthesis of pure lead sulfide (PbS) and Ag-doped PbS for photovoltaic applications. Nanotechnology Reviews 10 (1), 1484–1492.

Jameel, M.H., Agam, M.A., Hamzah, M.Q., Roslan, M.S., Rizvi, S.Z. H., Yabagi, J.A., 2021. Structural, optical and morphological properties of. Digest Journal of Nanomaterilas and Biostructures 16 (2), 399–408.

Khorsand, A., Suhaili, N., Aziz, A., Manaf, A., Kordi, F., 2016. XPS and UV – vis studies of Ga-doped zinc oxide nanoparticles synthesized by gelatin based sol-gel approach. Ceram. Int. 42 (12), 13605–13611.

R. Kumar and R. K. Choubey, "Study of Nonlinear Refraction of Organic Dye by Z-scan Technique Using He – Ne Study of nonlinear refraction of organic dye by Z-scan technique using He – Ne laser," *In AIP Conference Proceding,* vol. 1512,no.1,pp 470-471. February, 2013.

S. Kumar, T. Kang, and R. K. Singh, "Structural and optical properties of silica capped ZnS : Mn quantum dots Structural and optical properties of silica capped ZnS : Mn quantum dots," *Journal of materials Science: Materials in Electronics*, vol.no. 26.pp 3939-3946, June, 2015.

Kumar, S., Jeon, H.C., Kang, T.W., Seth, R., Panwar, S., Shinde, S. K., Waghmode, D.P., Saratale, R.G., Choubey, R.K., 2019. Variation in chemical bath pH and the corresponding precursor concentration for optimizing the optical, structural and morphological properties of ZnO thin films. J. Mater. Sci.: Mater. Electron. 30 (19), 17747–17758.

Kumar, Y., Sahai, A., Olive-méndez, S.F., Goswami, N., Agarwal, V., 2016. Morphological transformations in cobalt doped zinc oxide nanostructures : Effect of doping concentration. Ceram. Int. 42 (4), 5184–5194.

Mohamed, A.A., Khairalla, B.M., 2019. A Computer Simulation of Lithium Doped in nanosheet zinc oxide. Journal of the Faculty of Science and Technology 6, 110–116.

Mondal, S., Kanta, K.P., Mitra, P., 2013. Preparation of ZnO Film on p-Si and I-V Characteristics of p-Si / n-ZnO. Mateerials Research 16 (1), 94–99.

Nava, O.J., Luque, P.A., Olivas, A., 2017. In fl uence of Camellia sinensis extract on Zinc Oxide nanoparticle green synthesis. J. Mol. Struct. 1134, 121–125.

Ozel, K., Yildiz, A., 2021. High-detectivity ultraviolet-B photodetector based on SnO2 thin film/Si heterojunction. Semicond. Sci. Technol. 36, (9) 095001.

S. Panwar, T. Kang, S. Kumar, and R. K. Choubey, "Effect of zinc oxide concentration in fluorescent ZnS : Mn / ZnO core – shell nanostructures Effect of zinc oxide concentration in fluorescent ZnS : Mn / ZnO core – shell nanostructures," *Journal of Materials Science: Materials in Electronics*, vol.no.25, pp 1716-1723, April, 2014.

Parra, M.R., Haque, F.Z., 2014. Aqueous chemical route synthesis and the effect of calcination temperature on the structural and optical

properties of ZnO nanoparticles. Integrative Medicine Research 3 (4), 363–369.

Prasad, S., Raj, H., Joo, H., Hee, C., 2015. Deposition of ZnO fl owers on the surface of g-C 3 N 4 sheets via hydrothermal process. Ceram. Int. 41 (10), 12923–12929.

Ragupathi, C., Vijaya, J.J., Narayanan, S., Jesudoss, S.K., Kennedy, L.J., 2015. Highly selective oxidation of benzyl alcohol to benzaldehyde with hydrogen peroxide by cobalt aluminate catalysis: A comparison of conventional and microwave methods. Ceram. Int. 41 (2), 2069–2080.

Raja, G., Ragupathi, C., Sivaraman, G., 2019. Relative Role of Particle Size and Shape on the Magnetic and Catalytic Behavior of Nanozinc Chromite. J. Supercond. Novel Magn. 32 (5), 1451–1457.

Rajesh Kumar, B., Hymavathi, B., 2017. X-ray peak profile analysis of solid-state sintered alumina doped zinc oxide ceramics by Williamson-Hall and size-strain plot methods. J. Asian Ceram. Soc. 5 (2), 94–103.

Singh, A., Islamia, J.M., Choubey, R.K., November 2020. Manganese-Doped ZnS QDs : an Investigation into the Optimal Amount of Manganese-Doped ZnS QDs : an Investigation into the Optimal Amount of Doping. Semiconductor 54, 1450–1458.

Srivastava, V., Gusain, D., Sharma, Y.C., 2013. Synthesis, characterization and application of zinc oxide nanoparticles. Ceram. Int. 39 (8), 9803–9808.

Vafaee, M., Ghamsari, M.S., 2007. Preparation and characterization of ZnO nanoparticles by a novel sol – gel route. Materials Letters 61, 3265–3268.

Vijayakumar, S., Mahadevan, S., Arulmozhi, P., Sriram, S., Praseetha, P.K., 2018. Materials Science in Semiconductor Processing Green synthesis of zinc oxide nanoparticles using Atalantia monophylla leaf extracts : Characterization and antimicrobial analysis. Mater. Sci. Semicond. Process. 82 (March), 39–45.

Vijayaprasath, G., Murugan, R., Hayakawa, Y., Ravi, G., 2016. Optical and magnetic studies on Gd doped ZnO nanoparticles synthesized by co-precipitation method. J. Lumin. 178, 375–383.

Wahab, R., Ansari, S.G., Kim, Y.S., Dar, M.A., Shin, H., 2008. Synthesis and characterization of hydrozincite and its conversion into zinc oxide nanoparticles. Journals Alloys and Compounds 461, 66–71.

Yedurkar, S., Maurya, C., Mahanwar, P., 2016. Biosynthesis of Zinc Oxide Nanoparticles Using Ixora Coccinea Leaf Extract — A Green Approach. Open Journal of Synthesis Theory and Applications, 1–14.

Yildiz, Z.K., Atilgan, A., Atli, A., Özel, K., Altinkaya, C., Yildiz, A., 2019. Enhancement of efficiency of natural and organic dye sensitized solar cells using thin film TiO2 photoanodes fabricated by spin-coating. J. Photochem. Photobiol., A 368, 23–29.

Zaman, A., Uddin, S., Mehboob, N., Ali, A., 2020. Structural investigation and improvement of microwave dielectric properties in Ca (HfxTi1-x) O3 ceramics. Phys. Scr. 96, (2) 025701.

Zaman, A., Uddin, S., Mehboob, N., Ali, A., Ahmad, A., Bashir, K., 2021. Effect of Zr4+ on the structural and microwave dielectric properties of CaTiO3 ceramics. Ferroelectrics 577 (1), 143–152.